Reflection-type single long-pulse solar simulator for high-efficiency crystalline silicon photovoltaic modules

Binxin Hu,[1,a)] Buyin Li,[1] Rixin Zhao,[2] and Tiechen Yang[2]
[1]*Department of Electronic Science and Technology, Huazhong University of Science and Technology, Wuhan 430074, China*
[2]*Wuhan Gobo Photoelectric Technology Co., Ltd, Wuhan, 430223, China*

(Received 9 March 2011; accepted 18 May 2011; published online 13 June 2011)

Photovoltaic module measurements are predominantly taken by using pulsed solar simulators. However, significant errors can be generated when the existing simulators are applied to current high-efficiency crystalline silicon photovoltaic modules. This paper presents the design and implementation of a novel solar simulator featuring reflection-type light source and single long-pulse flash. The analysis and experimental study of the capacitance effect and the technical details of the simulator including reflection-type lamp house, xenon flash lamp power supply, and source-measure unit are introduced. The results show that the complete system achieves Class AAA performance in accordance with the international standard. The proposed simulator outperforms other similar products on the market and has been adopted by some well-known photovoltaic module manufacturers. The practical application demonstrates that this high-performance and cost-effective simulator is quite suitable for photovoltaic module production line. © *2011 American Institute of Physics*. [doi:10.1063/1.3598343]

I. INTRODUCTION

So far, crystalline silicon (c-Si) photovoltaic (PV) still makes up more than three-fourths of the module market and this leadership is expected to continue. This is based on the advantages of high efficiency, material abundance, technology maturity, and material non-toxicity.[1] In order to further expand the use of PV modules, it is necessary to thoroughly reduce the power-generating cost. With this goal, technologies for higher efficiency and thinner wafer both are important. As for the higher efficiency, numerous manufacturers have put in a great deal of effort. Currently, there are two leading high-efficiency c-Si solar cells with an efficiency of ∼22% or more that are under mass production, namely, the Back-Contact solar cell of Sun Power and the HIT cell of Sanyo Electric.[2–4] Their production in 2009 was 653 MW and is expected to hit 900 MW in 2010. Nevertheless, this market continues to keep a rapid growth: some other top producers, including Suntech, Yingli, and JA, have decided to join this team in 2010.[5,6]

The solar simulators used for PV module testing are commonly operated in a pulsed mode (as opposed to steady-state mode) to minimize electrical power consumption, module heating during test, and maximize the time between required lamp changes. The pulsed solar simulators can be further subdivided into single long-pulse (SLP) systems acquiring the total current voltage (I-V) characteristic during one flash and short multi-pulse systems acquiring one I-V data point per flash. The industry trend is moving toward SLP rather than multi-pulse for several reasons, including faster test time, higher throughput, the use of high-efficiency c-Si solar cells, and reduced sensitivity to various solar cell physical phenomena.[7] For most pulsed solar simulators on the market in the 2010s, typical pulse duration is in the order of milliseconds or less.[8] It is well known that using pulsed light sources for the I-V characterization of high-efficiency c-Si PV modules, special precautions must be taken to ensure an accurate measurement. In the past, efforts were made to develop correction procedures for transient I-V measurements.[9–12] Nowadays, the impact of transient errors can be problematic when the existing pulsed solar simulators are applied to current high-efficiency c-Si PV modules. Although it is expected that longer pulse duration may be required for those PV modules, the quantitative effect is not well understood; besides, the practicable tools are seldom commercially available at present.

Three of the most important specifications involved in determining a solar simulator are spectral match, spatial uniformity and temporal stability. Of these specifications, the one that has traditionally been the hardest to satisfy is the spatial uniformity. Numerous developers have to resort to complicated collimating optical system.[13,14] The other one that has been quite difficult to ensure is the temporal stability. A long-standing method of lamp irradiance control involves regulating a linear regulator (i.e., power MOSFET), thereby altering the voltage that is applied across the energy-storage capacitor.[15] This method suffers from low efficiency and occupies large volumes. Also, it is not really suitable for higher-power applications. The source-measure unit (SMU) with both measuring and sourcing capabilities is another huge technical challenge. An alternative solution requires an external programed control electric load and a plug-in data acquisition board.[16] Although these components can be ordered from market, they are vendor-defined and uneconomical. To the best of our knowledge, only a few leading firms (i.e., Spire and Berger) investigate the capacitance effect and provide the SLP systems, which are often expensive and irreplaceable. However, due to the technical monopoly, the related technical details have not been published or reported. Moreover, enormous PV module assemblers with low profits can hardly afford such tools, thus indirectly affecting the popularization of

a)Electronic mail: bxhu@smail.hust.edu.cn.

high-efficiency modules. Realizing this, we undertake a major effort to develop a high-performance, cost-effective SLP system with our own intellectual property rights. This is the GSMT-H as presented in this paper.

In this work, the capacitance effect is analyzed theoretically. The quantitative effect related to pulse duration is determined by experiment. The pulse duration is extended to 100 ms and measurements in constant voltage (CV) and constant current (CC) modes overlap optimally, thus maximizing efficiency and minimizing negative effects. An original reflection-type lamp house is provided to obtain high spatial uniformity. An improved xenon flash lamp (XFL) power supply is introduced to ensure a more uniform and predictable irradiance. A stand-alone SMU is designed to improve the I-V measurement. The complete system has been calibrated by National Institute of Metrology. The calibration certificate validates Class AAA performance for IEC60904-9: 2007. This SLP system has been adopted by some well-known PV module manufacturers in the world. The practical application demonstrates that this system is quite suitable for PV module production line. Although this system is designed for high-efficiency c-Si PV modules, it can be applicable to various thin-film PV modules such as a-Si, CdTe, or CIGS.

II. THEORY AND METHODS

A. Capacitance effect

At the heart of any solar cell is the PN junction, where there exists the diffusion capacitance C_d and the depletion-layer capacitance C_j. As the junction is always forward biased, C_j can be neglected. Our interest lies only in C_d, which results from the effect of the excess minority carriers stored in the quasi-neutral region of a diode. This charge is compensated by an equal quality of excess majority carriers drawn from the opposite side of the junction. For a time-dependent photocurrent induced by an irradiation pulse, the excess minority charge must change, implying a capacitive effect. C_d can be expressed as[17]

$$C_d = \frac{q}{kT} \cdot \frac{I_d}{1/\tau_h + 1/\tau_B}, \tag{1}$$

where I_d is the current through the junction, τ_h is the lifetime of the minority carriers, τ_B is the total transient time of the carriers across the diode and T is the absolute device temperature. τ_B is obviously infinite if the solar cell base width ω is much larger than the diffusion length L_n of the excess minority carriers. C_d is directly proportional to the product of τ_h and I_d and inversely proportional to the thermal voltage V_T and can, therefore, be written as

$$C_d = \frac{\tau_h}{V_T} \cdot I_d. \tag{2}$$

The minority carrier lifetime of high-efficiency cells is as high as several milliseconds. They can show a diffusion capacitance in the range of some μF.[18] In these cases, the effects of high capacitance have to be taken into account. Figure 1 depicts the equivalent circuit of a solar cell including

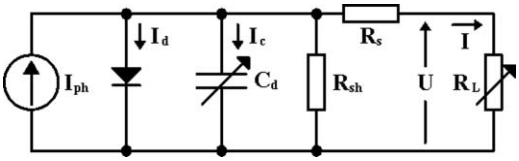

FIG. 1. Equivalent circuit of a solar cell.

a parallel bias-dependent capacitance. It can partially explain the capacitance effect.

The discrepancy between quasi-steady-state and transient measurements is due to the capacitive current I_c, which must be either added to or subtracted from the photocurrent I_{ph} depending on the measurement conditions. When the bias voltage rises (reduces) rapidly, the carrier concentration also increases (decreases) quickly, meanwhile, the cell capacitance must be charged (discharged) which results in a smaller (larger) cell current as measured under transient conditions. I_c is defined as

$$I_c = C_d \frac{dU_d}{dt} + U_d \frac{dC_d}{dt}. \tag{3}$$

For the ease of analysis, the shunt resistance R_{sh} and the series resistance R_s are neglected and hence the voltage across the diode U_d is equal to the voltage across the load U. From Eqs. (2) and (3) and the Diode Equation, I_c can be written as

$$i_c(t) = \frac{\tau_h I_0}{V_T}\left[\exp\frac{v(t)}{nV_T}\left(1 + \frac{v(t)}{nV_T}\right) - 1\right]\frac{dv(t)}{dt}, \tag{4}$$

where $v(t)$ is the bias voltage, n is the emission factor, and I_0 is the reverse saturation current. Taking the I-V transient measurement, when the sweep direction is forward (reverse), I_c is positive (negative) and must be subtracted from (added to) I_{ph}. Thus, either the maximum power $P_{\max}$ or the fill factor FF will get smaller (larger) than that measured under quasi-steady-state conditions. Negative effects are more significant as the sweep time becomes shorter.

B. Quantitative effect

The Sanyo HIT Power 190 PV module ($P_{\max}$ ~190 W, efficiency ~16.4%, FF ~0.75, area ~1.16 m^2) is chosen as the test specimen. I-V characteristics are measured under Standard Test Conditions (STC: 1,000 W/m^2 irradiance, 25 °C module temperature and AM1.5G spectrum) by the SLP system in this work. The pulse duration ranges from 10 ms to 100 ms. Linear voltage sweep is performed in the forward and reverse directions. Figure 2 shows the results of the P-V curves and FF variation curve at different pulse duration.

It is clear that $P_{\max}$ and FF are greatly dependent on the pulse duration and the sweep direction. The deviation closely rises at an exponential rate with the pulse duration decreasing. If the pulse duration is not more than 30 ms, the deviation is up to 10% or more. As the pulse duration approaches 80 ms, the deviation reduces to 1% or less. These results agree with the said ideas related to the capacitance effect. There is a trade-off between pulse duration and energy consumption.

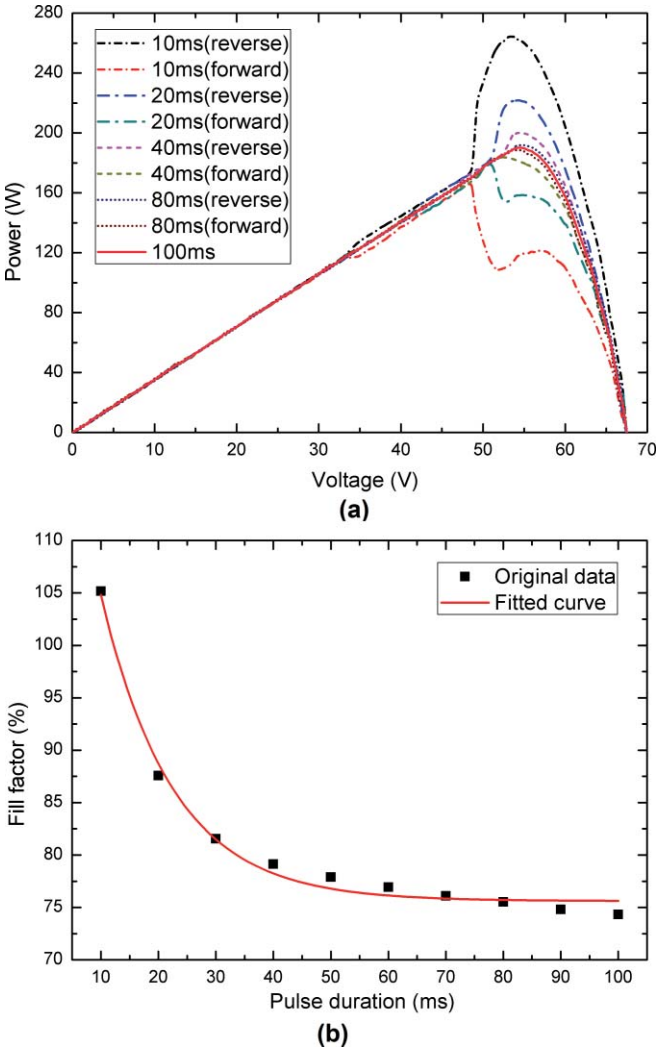

FIG. 2. (Color online) P-V curves (a) and *FF* variation curve (b).

The pulse duration is, therefore, set to 100 ms for precisely characterizing these high-efficiency modules.

C. Sweep mode

Linear voltage sweep is popular in the I-V measurement.[19] However, it appears to be inefficient and unbalanced. As shown in Fig. 3, more than 80% range of sweep voltage (0 V to $V_{\max}$) merely results in less than 20% changes of current (I_{SC} to $I_{\max}$).

An improved sweep mode revolves switching the operation mode of the SMU in accordance with I-V characteristics of a PV module. When the voltage is within $V_{\max}$ to V_{oc}, the SMU will be operated in CC mode. When the current is within $I_{\max}$ to I_{SC}, the SMU will be operated in CV mode. Measurements in CC and CV modes overlap optimally to maximize efficiency and minimize negative effects.

III. SYSTEM IMPLEMENTATION

As shown in Fig. 4, the SLP system consists of the following functional units: lamp house, XFL power supply, thermometer, reference cell, electronic load, DAU, IPC, and CAN network.

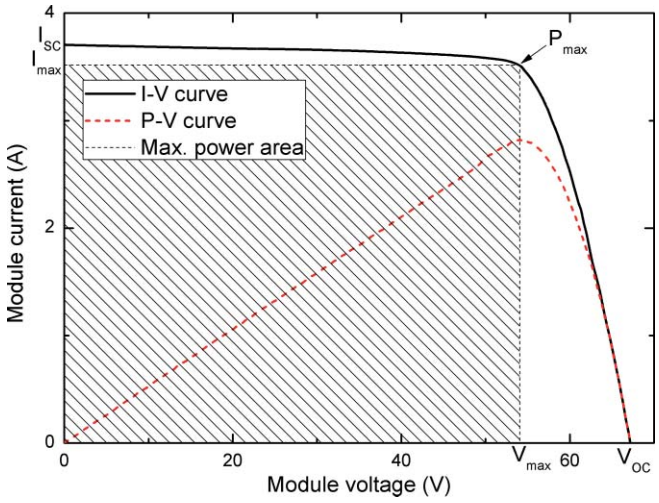

FIG. 3. (Color online) I-V characteristics of a PV module.

Electronic load and DAU are integrated into a stand-alone SMU, which is connected to the terminals of the specimen by using four-wire method. XFL power supply, SMU, and IPC communicate through CAN network, which has the advantages of anti-jamming ability, high-speed, remote connection, multimaster and maintenance free. IPC running virtual front panel serves as the display console, which is linked to CAN network through a USB to CAN intelligent adapter.

The C8051F060 mixed-signal System-on-a-Chip (SoC) MCU is chosen as a core processor of the XFL power supply and the SMU because of its high integration and low cost. It combines high performance with first-class peripherals, such as a CAN2.0B controller, two separate 16-bit 1Msps ADCs and two separate 12-bit DACs, thus providing a complete data acquisition or control system solution.

The reference cell that tracks the instantaneous irradiance in the test plane triggers the I-V measurement. The noncontact infrared thermometer monitors the temperature of the specimen. If this temperature is not the desired temperature, the measured I-V characteristic should be corrected in accordance with IEC60891: 2009.

A. Reflection-type lamp house

As shown in Fig. 5, the reflection-type lamp house contains four components: cabinet **1**, XFL **4**, bracket **9**, and cover

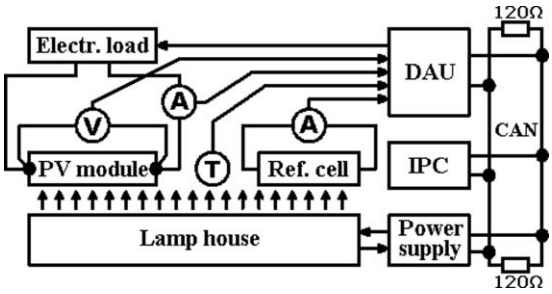

FIG. 4. Block diagram of the SLP system.

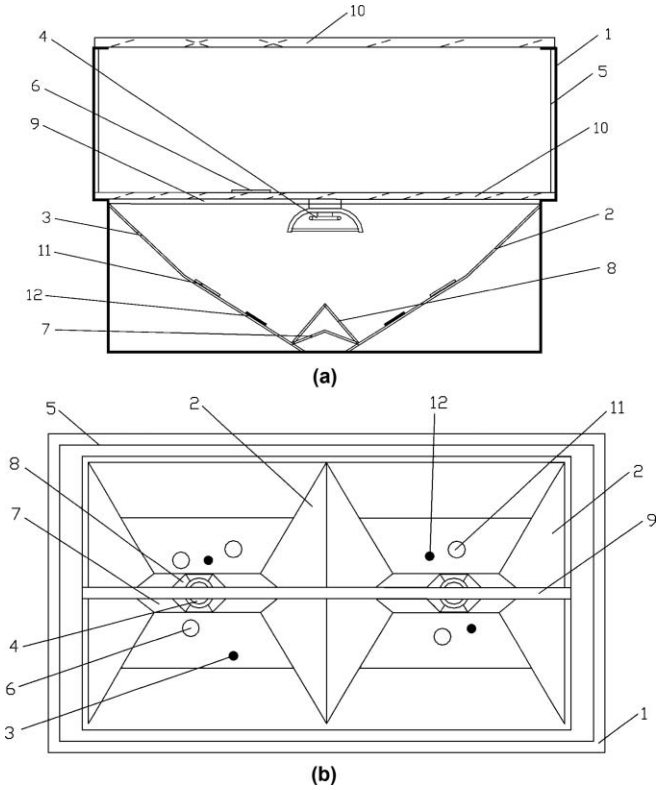

FIG. 5. Configuration of the lamp house: section view (a) and vertical view (b).

glass **10**. The main parts of the cabinet are dipper-form body **2**, rectangle shell **5**, embossment **7**, and hexagonal pyramid 8. The other parts contributing to the spatial uniformity are pore hole **3**, translucent sheet **6**, reflective sheet **11**, and opaque sheet **12**.

The basic material constructing the cabinet is the reflective plate that is made of alloy AlMn1Cu (EN AW 3003) and has received special surface treatments of sand blasting and oxidation to reinforce the diffuse reflection, yielding a reflectivity of ∼90% over the visible spectrum. So many reflective plates are seamlessly connected and contribute most to the spatial uniformity.

The upper part of the cabinet is the rectangle shell made up of four reflective plates. The lower part of the cabinet is divided into two identical dipper-form bodies. Each body is made up of four reflective plates. These plates slope at an angle of ∼45° to the underside of the cabinet. At the bottom of the dipper-form body, there is the embossment including two reflective plates. A couple of appropriately fitted XFLs serve as light sources. Each XFL is over the dipper-form body and is firmly fixed to the bracket. Under the XFL and on the embossment, there is the hexagonal pyramid made up of six reflective plates. These plates slope at an angle of ∼60° to the underside of the cabinet.

There are two cover glasses. One is on the bracket for protecting internal components while the other is on the rectangle shell for bearing the test specimen. The test plane is 2.0 m long and 1.2 m wide. Some reflective (opaque) sheets are stick on the dipper-form body to strengthen (weaken) the reflection effect. Their location and size depend on the irradiance measured in the making. They generally locate where there is a higher (lower) irradiance. To the benefit of the spatial irradiance, some pole holes are bored in the dipper-form body and a few translucent sheets are stick on the lower cover glass. They all locate where there is a higher irradiance. Their location and size also rests with the irradiance measured in the making.

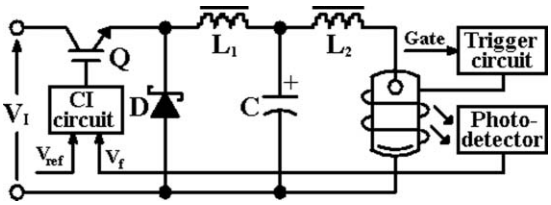

FIG. 6. Scheme of the power supply.

B. XFL power supply

The SLP system is equipped with two identical power supplies, which utilize a heavy duty XFL and AM1. 5G calibrated solar filter to approximate the sun's true spectral distribution, respectively. The two power supplies are controlled by a SoC MCU. The scheme of the power supply is illustrated in Fig. 6.

Upon initiation of a flash command, the lamp is energized by application of the trigger circuit, while the reference voltage V_{ref} is set to a desired level. The constant irradiance (CI) circuit, having sensed that the feedback voltage V_f is too low, switches on the pass transistor Q to build up current in the inductor L_1, which also starts to charge capacitor C. The voltage across the lamp rises to a critical level that is referred to as its minimum strike voltage, thus firing the lamp. If V_f is larger than V_{ref}, the pass transistor Q turns on, and the capacitor C discharges through the lamp. The energy stored in the inductor L_1 is also transferred to lamp. If V_f is less than V_{ref}, the pass transistor Q turns off to build up current in L_1, and the capacitor C is recharged. This self-regulation is repeated until the total duration required by the lamp is realized.

The photodetector converts the instantaneous irradiance to a proportional feedback voltage V_f. The SoC MCU generates a reference voltage V_{ref} via its built-in 12-bit DAC. The close irradiance regulation provided by the constant irradiance (CI) circuit ensures a more uniform and predictable irradiance for each flash. The pass transistor (i.e., IGBT) is operated in switching mode rather than in linear mode to maximize efficiency and minimize volumes. The discharge choke L_2 limits the rate at which the discharge current passes through the xenon lamp to establish the duration and irradiance of the flash.

The reference voltage determines the two crucial parameters of each flash. The irradiance is linear in its level. The pulse duration is proportional to its width. Figure 7 shows that the irradiance can be selected by changing the level of the reference voltage. This circuit can provide an irradiance range of 200 W/m^2 to 1,200 W/m^2 and a pulse duration range of 10 ms to 100 ms. The setting time is less than 500 μs.

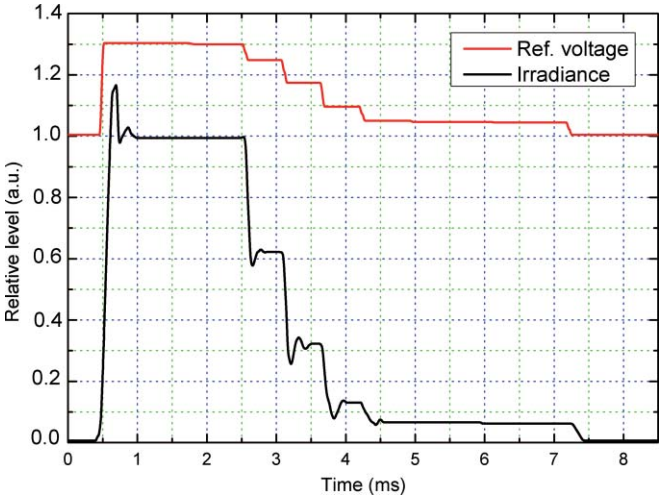

FIG. 7. (Color online) Irradiance vs. Reference voltage.

For a given flash lamp power supply, there are two values which determine the specific design and circuit components, namely, the stored energy E_0 and the 1/3 current pulse width Γ. They are derived from the following equations:

$$E_0 = \frac{1}{2} C V_0^2, \tag{5}$$

where C is the main discharge capacitor and V_0 is the dc charge voltage,

$$\Gamma = \pi \sqrt{LC}, \tag{6}$$

where L is the pulse shaping inductor.

From the above equations, the power supply size and cost can be further reduced by using smaller C and L. For illustrative purposes, it is assumed that the pulse duration is 100 ms, the irradiance is 1,000 W/m^2, the test area is 1.0 m by 1.2 m and the energy conversion efficiency is 40%. Thus, the power supply is to supply 300 joules of energy to flash lamp. The dc charge voltage V_0 is 380 V, and the switching period is 0.1ms. The capacitor supplies 0.3 joules per period then the capacitor has a value of 1/10 of the typical capacitance associated with this energy requirement of 300 joules or 470 μF for the capacitor C. The value of inductor L is chosen as 120 μH. Although the instantaneous power is as high as 3000 W, the average power is only 10 W on the condition that the XFS flashes every 30 s.

C. Source-measure unit

Figure 8 shows the scheme of the SMU, which has four separate data input lines that simultaneously store values of current, voltage, irradiance, and temperature. There is a hardware structure of dual core processor. The primary processor takes I-V measurements and the secondary processor records the variation of irradiance and temperature. Both processors work synchronously and own the same ID in the CAN network.

The voltage across the test specimen is attenuated to the desired range by a difference amplifier. The divider ratio, either 0.03 or 0.3, is selected by switching between two 0.1%,

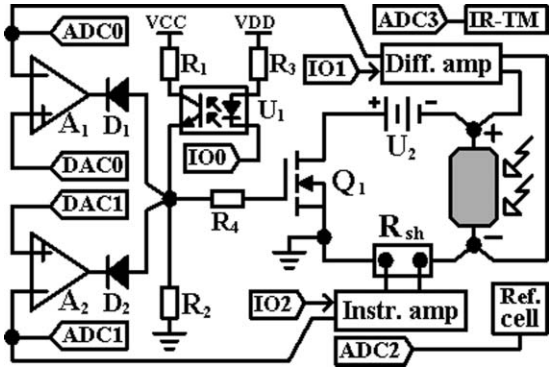

FIG. 8. Scheme of the source-measure unit.

15 ppm/°C precision resistors. They are 4.3 kΩ and 15 kΩ. The resulting signal is then applied to the inverting terminal of an op-amp A_1 and enters the ADC0. The current flows through a 1%, 5 W, and 30 mΩ shunt resistance. The resulting voltage drop is amplified to the desired range by a monolithic in-amp. The internally preset gains of 10 and 100 are pin-selectable, with 5 ppm/°C gain drift. The amplified signal is then applied to the inverting terminal of an op-amp A_2 and enters the ADC1. A trigger signal from the reference cell is directly connected to the ADC2. The REF5030 ultrahigh precision reference is used to ensure a better accuracy on low voltage inputs.

The DAC0 and DAC1 are initialized to 0 V and V_{ref}, respectively, in preparation for the short-circuit current measurement. When a flash event happens, the ADC2 will be outside the desired range, thus triggering the I-V measurement. As the optical isolator U_1 is initially disabled, the open-circuit voltage V_{oc} is measured and stored. The optical isolator U_1 is then enabled. The short-circuit current I_{sc} is also measured and stored. In CV mode, the DAC0 output starts at 0 V and stops at *Voc/K*, where *K* is divider factor. Owing to the effect of negative feedback, the voltage increases with the DAC0 output. In CC mode, the DAC1 output starts at 0 V and stops at $I_{qsc} \cdot G$, where G is total gain. Likewise, the current increases with the DAC1 output. Because only one of the two isolation diodes D_1, D_2 takes effects at any time, the two sweep modes are mutually independent. The power MOSFET Q_1 operates in the triode region acting as active variable resistor, thereby regulating either current or voltage in accordance with the sweep mode. The bias voltage source U_2 is used to offset the voltage drop across the external series resistance, thus ensuring that the short-circuit current is measured at zero voltage. The bias voltage is set to 3V and is greater than the voltage drop.

IV. RESULTS

A. Spectral match

Spectral irradiance of this simulator has been measured by Konica Minolta S-2442 Soma spectroradiometer, which features a wavelength of 300–1100 nm, 5 nm resolution, and 1–1000 ms exposure time. The simulator operates under STC

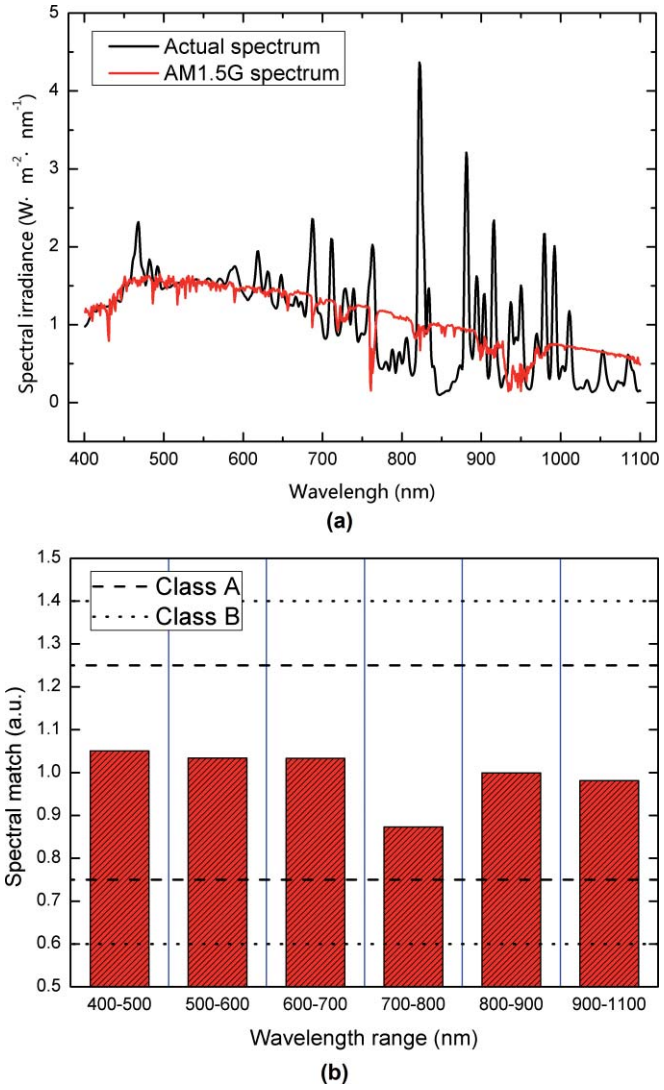

FIG. 9. (Color online) Spectral output: spectral distribution (a) and spectral match (b).

while the pulse duration is set to 100 ms. The wavelength range is restricted from 400 nm to 1100 nm.

Figure 9 shows the spectral distribution over the restricted bands and the spectral match to AM1.5G for six wavelength intervals of interest. The maximum and minimum spectral match are 1.05 (400–500 nm) and 0.87 (700–800 nm), respectively, thus leading to a Class A simulator for spectral match.

B. Spatial non-uniformity

Spatial non-uniformity of the irradiance is given by

$$S_{N,E}(\%) = \frac{E_{t,\max} - E_{t,\min}}{E_{t,\max} + E_{t,\min}} \times 100\%, \tag{7}$$

where $E_{t,\max}$ and $E_{t,\min}$ are the maximum and minimum total irradiance, respectively, measured with a reference cell over the test plane.

The test plane is divided into 64 equally sized test positions. The desired irradiance is 100 mW/cm^2. Figure 10 shows the general distribution of total irradiance measured over the test plane. $E_{t,\max}$ and $E_{t,\min}$ n are 101.22 mW/m^2 (x = 62.5 cm, y = 67.5 cm) and 98.44 mW/m^2 (x = 162.5 cm, y = 97.5 cm), respectively. $S_{N,E}$ is calculated as 1.39%, thus achieving Class A for non-uniformity of spatial irradiance.

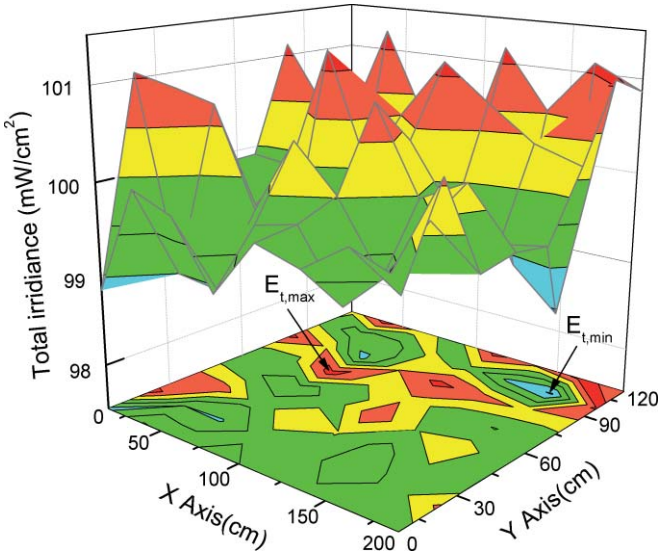

FIG. 10. (Color online) Distribution of total irradiance.

C. Temporal instability

Temporal instability of the irradiance is given by

$$T_{I,E}(\%) = \frac{E_{t,\max} - E_{t,\min}}{E_{t,\max} + E_{t,\min}} \times 100\%, \tag{8}$$

where $E_{t,\max}$ and $E_{t,\min}$ are the maximum and minimum total irradiance, respectively, measured with a reference cell during a single measurement plateau.

Owing to synchronous data acquisition, the temporal instability is Class A for the short term instability (STI). The long term instability (LTI) is a major concern. Tests are carried out under standard (1000 W/m^2) and low (100 W/m^2) irradiances. The pulse duration is set to 100 ms. Figure 11 shows the irradiance variation of measured data set during the

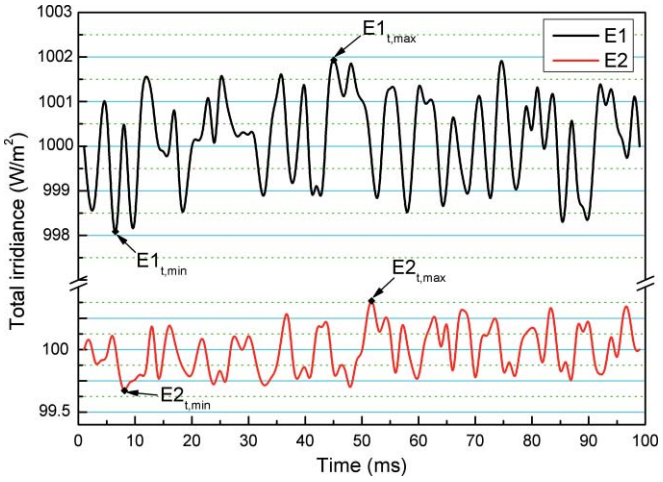

FIG. 11. (Color online) Irradiance variation during the plateau.

TABLE I. Results of static calibration.

Item	Range	Resolution	Accuracy	Uncertainty ($k = 2$)
dc	10 V	1mV	0.04%	0.06%
Voltage	100 V	10 mV		
dc	1 A	100 μA	0.08%	0.10%
Current	10 A	1 mA		

98 ms plateau. The LTI achieves 0.19% under standard irradiance and 0.36% under low irradiance. All along the plateau, the Class A requirement is met.

D. Measurement capabilities

The Fluke 5700A/5720A multi-function calibrator is used to calibrate the built-in DAU. The calibration items include dc voltage and dc current. The results of calibration are shown in Table I. The accuracy of measurement is better than 0.1% for both items with four digit resolution. Table I also gives the measurement uncertainty of each item, which is expressed as the related expanded uncertainty.

To examine the repeatability of dynamic test, ten repeated measurements are applied to a HIT Power 190 PV module under STC. The parameters related to maximum power point come into focus. Figure 12 shows the variation trend of dynamic test. The deviation factor of each measurement is within ±0.1%. The repeatability is expressed as the relative standard deviation. The repeatability for I_{max} and V_{max} are calculated as 0.04% and 0.01%, respectively.

E. Practical application

Some well-known PV module producers such as Sanyo, Kyocera, Yingli, and Jiawei (an assembly partner of SunPower) have adopted this SLP system. The practical application demonstrates that this system is particularly suitable for PV module production line. Table II summarizes the performance comparison between the GSMT-H and three typical pulsed solar simulators available in the market.[20–22]

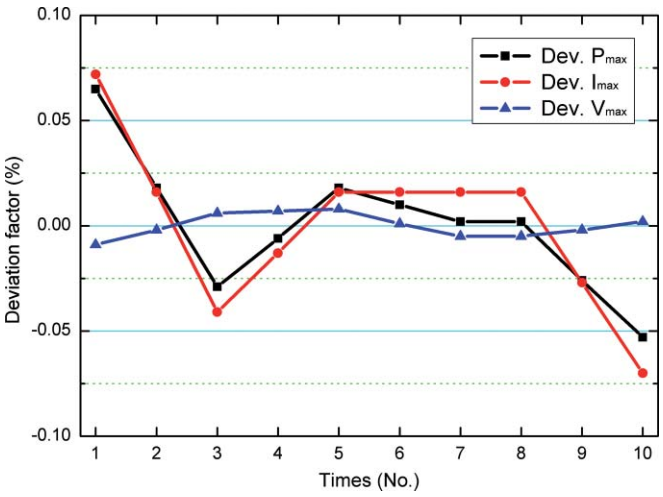

FIG. 12. (Color online) Variation trend of dynamic test.

TABLE II. Comparison with other simulators.

Item	4600SLP (Spire)	PSS 8 (Berger)	WPSS (Wacom)	GSMT-H
Illuminated area (cm^2)	200 × 137	200 × 130	120 × 100	200 × 120
Irradiance range (sun)	0.4–1.1	0.5–1.1	0.8–1.2	0.2–1.2
Pulse duration (ms)	20–80	10	80	10–100
Spectral match	0.75–1.25	0.75–1.25	0.75–1.25	0.87–1.05
Spatial uniformity (%)	±2	±2	±3	±1.4
Temporal stability (%)	±0.2	±1	±1	±0.2

It can be seen from Table II that the performance of the GSMT-H surpasses that of other products in several key specifications. Most importantly, the desired results are obtained at a lower cost. This high-performance and cost-effective system has been one of the leading photovoltaic testing tools in the market.

V. CONCLUSIONS

To cope with the increasing high-efficiency c-Si PV modules, a novel solar simulator featuring reflection-type light source and single long-pulse flash has been developed. The analysis and experimental study of the capacitance effect indicate that negative effects can be excluded when the pulse duration is extended to 100 ms and measurements in CV and CC modes overlap optimally. The proposal of this paper is to use the reflection-type lamp house and the switching-mode XFL power supply to obtain a more uniform and predictable optical output (irradiance). The results show that the proposed simulator achieves a Class AAA performance in accordance with IEC 60904–9: 2007. Equipped with a well-designed SMU, the complete system provides better than 0.1% accuracy for I-V measurements and realizes automatic correction for irradiance and temperature. Owing to wide-range irradiance and pulse duration, this SLP system reduces sensitivity to various solar cell physical phenomena and can be extended to different kinds of thin-film PV modules such as a-Si, CdTe, or CIGS. Additionally, the proposed methods and techniques can also be applied to any other measurement and control system used in industry field.

ACKNOWLEDGMENTS

This work was partly supported by the National Natural Science Foundation of China (Grant No. 60871017/F010612) and the Innovation Fund for Technology Based Firms of China (Grant No. 09C26154204984). The authors thank L. Lu and X. Jiang, NIM, who provided reliable calibration service.

[1] V. Petrova-Koch, R. Hezel, and A. Goetzberger, *High-efficient Low-cost Photovoltaics: Recent Developments* (Springer, Heidelberg, 2008).
[2] Y. Tsunomura, Y. Yoshimine, and M. Taguchi, Sol. Energy Mater. Sol. Cells **93**, 670 (2009).
[3] S. W. Glunz, Adv. OptoElectron. **2007**, 1 (2007).
[4] M. A. Green, K. Emery, Y. Hishkawa, and W. Warta, Prog. Photovoltaics. **19**, 84 (2011).

[5]Greentech Media, Inc. 2009 global PV Cell and Module production analysis, 2010.
[6]See http://www.greentechmedia.com for information about the firms that stand at the forefront of crystalline silicon efficiency, and their plans and products under the microscope.
[7]H. B. Serreze and R. G. Little, Photovoltaics International **1**, 1 (2008).
[8]M. Pravettoni, R. Galleano, E. D. Dunlop, and R. P. Kenny, Meas. Sci. Technol. **21**, 115901 (2010).
[9]G. Frieshen and H. A. Ossenbrink, Sol. Energy Mater. Sol. Cells **48**, 77 (1997).
[10]W. M. Keogh and A. W. Blakers, Prog. Photovoltaics. **12**, 1 (2004).
[11]C. Monokroussos, R. Gottschalg, A. N. Tiwari, G. Friesen, D. Chianese, and S. Mau, *IEEE 4th World Conf. on Photovoltaic Energy Conversion, Waikoloa*, 7–12 May 2006, Vol. 2, 2231.
[12]D. L. King, J. M. Gee, and B. R. Hansen, *Twentieth IEEE Photovoltaic Specialists Conf.*, Las Vegas, 26–30 Sept. 2008, Vol. 1, 555.
[13]H. B. Liu, Opt. Precis. Eng. (China) **9**, 177 (2001).
[14]R. X Zhao, C.N. patent 101,818,876 (2010).
[15]J. Wegrzyn, G. Patonay, and I. Warner, Rev. Sci. Instrum. **60**, 90 (1989).
[16]Y. Kuai and S. Yuvarajan, J. Power Sources **154**, 308 (2006).
[17]A. Bar-Lev, *Semiconductors and Electronic Device*, 3rd ed. (Prentice Hall, New York, 1993).
[18]A. Cuevas, M. J. Kerr, C. Samundsett, F. Ferrazza, and G. Coletti, Appl. Phys. Lett. **81**, 4952 (2002).
[19]Keithley Instruments, Inc., Understanding New Developments in Data Acquisition, Measurement, and control, 2007.
[20]See http://www.spirecorp.com for information about the 4600SLP that represents the latest simulation technology in the 2000s.
[21]See http://www.bergerlichttechnik.de for information about the PSS 8, which is a projection-type pulsed simulator and is characterized by huge test surface.
[22]See http://www.wacom-ele.co.jp for information about the WPSS that is a popular pulsed simulator on the east Asia market.